*J. Fluid Mech.* (1988), *vol.* 196, *pp.* 205–222
*Printed in Great Britain*



# On the wind force needed to dislodge a drop adhered to a surface

By PAUL A. DURBIN
NASA Lewis Research Center, Cleveland, OH 44135, USA

(Received 16 July 1987 and in revised form 7 April 1988)

The dislodging by dynamic pressure forces of a drop adhered by surface tension to a plane is analysed. An integro-differential equation describing the drop shape is solved numerically and the critical Weber number as a function of contact angle hysteresis is found.

## 1. Introduction

A drop of liquid sitting on a plane surface will be held in place by surface tension (Batchelor 1967, §1.9). In the absence of external forces, the drop assumes a symmetrical shape. If a force with component tangential to the surface is now applied, the drop will be distorted into an asymmetrical shape. As the magnitude of the force is increased, the drop will be increasingly distorted until surface tension is no longer able to hold the drop and it begins to slide along the surface: an example of this occurs when a sufficiently large drop of water is put on a smooth surface which is inclined with respect to gravity. When the inclination becomes large, the drop cannot be held by surface tension and it moves down the surface.

In the present paper, the perturbing force is the surface pressure associated with wind flow over the drop. This pressure field is itself a functional of drop shape, so that the drop distortion is described by an integro-differential equation. However, if the air flow is inviscid and remains attached, a symmetric drop will produce a symmetric surface pressure distribution; the drop will not be dislodged. In order to introduce asymmetry, our analysis will assume high-Reynolds-number free-streamline separation from the drop. The leeward side of the drop is then at constant pressure and the pressure field is asymmetrical. Because of the analytical difficulty of determining the separated flow field and of solving the governing integro-differential equation, we consider here two-dimensional slender drops.

The slender drop approximation entails replacing the normal to the drop by the normal to the solid surface: in many cases this is an adequate approximation. The restriction to two-dimensionality may be more discomforting, since most cases of interest involve three-dimensional drops. One expects the two-dimensional analysis to give some suggestion of what happens in three-dimensions because the forces governing the drop shape are the same. Its greater tractability also makes the two-dimensional case a useful preliminary to a more involved three-dimensional analysis and, of course, it applies to quasi two-dimensional drops.

By including only pressure forces, we are assuming that frictional drag can be ignored. This approximation must rely in some way on a high Reynolds number for its validity. The triple deck theory (Smith *et al.* 1981) shows that viscous and pressure forces become comparable when the drop height is of order $Re^{-\frac{1}{8}}$ times the

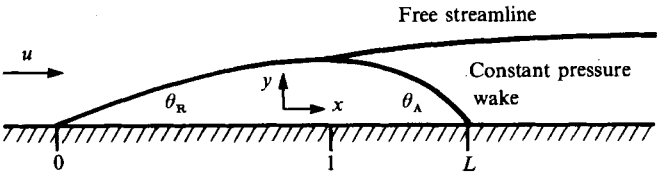


FIGURE 1. Defining sketch.

boundary-layer thickness; i.e. when the drop height is formally small compared to boundary-layer thickness. Therefore, the present analysis applies in the case when the drop height is comparable to, or greater than the boundary-layer thickness on the surface. This is the case in which the flow is severely separated, and form drag becomes predominant. Casual observation of water drops being blown off glass or mylar gives the impression that it is often true that the flow must be separated before a drag sufficient to dislodge the drop can be created. We intend to consider elsewhere the case of smaller drops for which pressure and viscous forces become comparable. The low-Reynolds-number limit, in which viscous surface stresses distort the drop, was considered by Dussan V. (1987).

Because our analysis is inviscid, an ambiguity exists in the location of the separation point. In the present paper, the separation point is taken as a free parameter. It was first described by Sychev (1972) and Smith (1977) how viscous effects could be introduced in order to determine the separation point unambiguously. In the present case, the thickness of the boundary layer approaching the drop would enter such a determination, and through this degree of freedom the separation point would remain a largely free parameter – viscous theory might conceivably place constraints on that freedom.

As in Dussan V.'s study, adherence to the surface is characterized here by contact angle hysteresis. Thus, the advancing and receding contact angles parameterize the cohesion of the liquid to the surface. These angles are determined by the nature of the liquid, the solid surface and the ambient air (Batchelor 1967). The wind will deform a static drop until the upwind contact angle has been decreased to the receding contact angle, $\theta_R$, and the downwind angle has been increased to the advancing contact angle, $\theta_A$ (figure 1). This is the critical drop configuration; a slightly greater wind speed will dislodge the drop. It is this critical configuration for which we obtain solutions. The critical wind speed is characterized by a critical Weber number:

$$w_V = \frac{\rho U^2 V^{*\frac{1}{2}}}{\sigma}, \tag{1}$$

where $\rho$ is the density of air; $U$ is the wind speed far from the surface; $\sigma$ is the surface tension at the air–liquid interface; and $V^*$ is the two-dimensional drop volume: obviously, for a three-dimensional drop the lengthscale would be $V^{*\frac{1}{3}}$.

## 2. Governing equations

We will take the origin to be at the leading edge of the drop, and it will prove convenient to use the position of separation, $x_s$, as our unit of length. At the end of the analysis we will revert to the lengthscale $V^{\frac{1}{2}}$ used in (1). The slender-body approximation, which linearizes the governing equations, results from taking $\bar{\theta} =$

$\frac{1}{2}(\theta_A+\theta_R)$ to be small. For this reason we scale the drop height, $\eta$, on $\bar{\theta}$. If superscript* denotes dimensional variables, then non-dimensional and dimensional quantities are related by

$$x=\frac{x^*}{x_s},\quad \eta(x)=\frac{\eta^*}{x_s\bar{\theta}},\quad V=\frac{V^*}{x_s^2\bar{\theta}},\quad P=\frac{P^*x_s}{\sigma\bar{\theta}}, \tag{2}$$

$P$ here is the constant pressure inside the drop: in the present high (air-flow) Reynolds-number limit, the lowest-order momentum balance inside the drop requires the internal pressure to be constant (see later discussion in §5).

In the critical configuration, a static balance exists between pressure and surface tension forces. Referring to figure 1, on the portion of the drop upstream of separation, the air pressure is determined by Bernoulli's equation, which is linearized in the slender-body approximation as $P_a=-Uu_s$, where $u_s$ is the surface velocity perturbation due to the drop. An expression for the Bernoulli pressure is derived in the Appendix. The rear of the drop is adjacent to a constant pressure wake, which in free-streamline theory is at the ambient pressure, $P_a=0$. The normal force on the drop surface is $P_a-P$, with $P$ the constant internal pressure: this internal pressure will be determined as part of the solution. The surface tension force which balances the pressure difference, is equal to the curvature of the drop times the surface tension coefficient. In the slender-body approximation this curvature is just $\mathrm{d}^2\eta/\mathrm{d}x^2$ (Batchelor 1967).

Upon introducing the notation $\xi(x)=\mathrm{d}\eta/\mathrm{d}x$, the equations governing droplet shape are

$$\frac{\mathrm{d}\xi}{\mathrm{d}x}=-P+\frac{w}{\pi}(1-x)^{\frac{1}{2}}\int_0^1\frac{\epsilon(x')}{(1-x')^{\frac{1}{2}}(x'-x)}\mathrm{d}x'\quad(0\leqslant x<1), \tag{3a}$$

$$\frac{\mathrm{d}\xi}{\mathrm{d}x}=-P\quad(L\geqslant x\geqslant 1), \tag{3b}$$

where $w=\rho U^2x_s/\sigma$ is the Weber number based on separation distance and the integral in (3$a$) is a Cauchy principal value (Muskhelishvili 1953). This integral simply determines the surface pressure produced by air flow over the portion of the drop upstream of separation. Because $P_a$ is zero within the separated wake (3$b$) obtains there.

A derivation of the expression for $P_a$ is given in the Appendix. It is shown there that (3) leads to the overall force balance

$$D=\frac{\rho U^2\bar{\theta}}{w}(\theta_A-\theta_R)$$

between surface contact and wind drag, $D$.

The surface height is given by

$$\eta(x)=\int_0^x\xi(x')\,\mathrm{d}x', \tag{4}$$

and the drop volume is

$$V=\int_0^L\eta(x)\mathrm{d}x, \tag{5}$$

where $L$ is the downstream end of the drop. Note that (see equation (1)) $w_v=w(V\bar{\theta})^{\frac{1}{2}}$ so that an evaluation of this last integral permits us to rescale our results on $V^{\frac{1}{2}}$ instead of the artifical length $x_s$.

The boundary conditions to (3) and (4) are that the drop height is zero at the downstream end of the drop,

$$\eta(L) = 0, \tag{6a}$$

and that the slope $\xi$ is equal to the receding (minus the advancing) contact angle at the upstream (downstream) end of the drop (see figure 1),

$$\xi(0) = 1-\epsilon, \quad \xi(L) = -1-\epsilon, \tag{6b,c}$$

where $\epsilon = (\theta_A - \theta_R)/2\bar{\theta}$ is the scaled contact angle hysteresis. As discussed in §1, the separation position is unknown, and regarded as a free parameter. Because it has been scaled out of our equations, this degree of freedom is replaced in the analysis by an indeterminate surface slope, $\xi_s$, at the separation point:

$$\xi(1) = \xi_s, \tag{6d}$$

$\xi_s$ enters our solution as a free parameter.

The problem posed in this section is to solve (3) for $\xi(x)$, $P$ and $w$ such that conditions (equations (6)) are satisfied. The curve $w(\epsilon)$ describes the critical Weber number dependence on contact angle hysteresis.

## 3. Solution

The solution to equation (3$b$) with (6$c$) is

$$\xi(x) = -1-\epsilon+P(L-x) \quad (L \geqslant x \geqslant 1) \tag{7}$$

and with (6$d$) one finds

$$L = 1+\frac{(1+\epsilon+\xi_s)}{P}. \tag{8}$$

This determines the drop length once the internal pressure has been found. The drop height in the separated region is found upon integrating (7) with (6$a$):

$$\eta(x) = (1+\epsilon)(L-x)-\tfrac{1}{2}P(L-x)^2 \quad (L \geqslant x \geqslant 1). \tag{9a}$$

Using (8), the height at separation is

$$\eta(1) = \frac{(1+\epsilon)^2-\xi_s^2}{2P}. \tag{9b}$$

Equation (9$b$) provides a boundary condition for the solution to (3$a$) in $0 < x < 1$. The scaled drop volume is

$$V = \int_0^1 \eta(x)\mathrm{d}x+\frac{(1+\epsilon+\xi_s)^2(1+\epsilon-\frac{1}{2}\xi_s)}{3P^2}, \tag{10}$$

after the contribution (equation (9$a$)) from the separated region is evaluated explicitly. Given this solution in $x \geqslant 1$, and its evaluation at $x = 1$, the droplet problem reduces to solution of equation (3$a$).

An integro-differential equation similar to (3$a$) is discussed by Muskhelishvili (1946, chapter 17). It appears from his discussion that no closed-form solution exists. For this reason, in the present paper numerical solution is resorted to. A brief, unsuccessful attempt at solution by a collocation method was abandoned in favour of a series expansion in powers of $w$. It was felt that this latter form of solution was more revealing.

Before proceeding with this expansion, let us rewrite (3*a*) as an integral equation for $\eta$. If first, (3*a*) is integrated from $x = 0$ to 1, it is found that

$$P = (1-\epsilon-\xi_s)+\frac{w}{\pi}\int_0^1 \frac{\xi(x)}{(1-x)^{\frac{1}{2}}}\left[2+(1-x)^{\frac{1}{2}}\ln\left(\frac{1-(1-x)^{\frac{1}{2}}}{1+(1-x)^{\frac{1}{2}}}\right)\right]dx. \tag{11}$$

Substituting this into (3*a*) and integrating that equation from $x$ to 1 gives an equation for $\xi$. If $x = 1-y^2$ is substituted, this equation is

$$\xi(y) = (1-\epsilon)y^2+\xi_s(1-y^2)-\frac{2w}{\pi}\int_0^1 \xi(y')\left[2(y-y^2)+y'\left(\ln\left|\frac{y-y'}{y+y'}\right|-y^2\ln\frac{1-y'}{1+y'}\right)\right]dy'. \tag{12}$$

Substitution of $-2y\xi(y) = d\eta(y)/dy$ and a further integration from $y$ to 1, yields an integral equation with $\eta$ as dependent variable. It is clear from the first two terms on the right-hand side of (12) that $\eta$ can be written as the sum of a term proportional to $\xi_s$ and one proportional to $(1-\epsilon)$. In our computations, $\eta$ was found by summing two such terms. However, for the purpose of presentation, no such separation will be made. Instead, we write $\xi_s = (1-\epsilon)s$, so that $s$ is the separation slope scaled on $\theta_R$, and introduce $h(y) = \eta(y)/(1-\epsilon)$. Then the integral equation governing the surface elevation can be written

$$h(y) = \tfrac{1}{2}(1-y^4)+\tfrac{1}{2}s(1-y^2)^2+\frac{4w}{\pi}\left(\frac{1-y^4}{4}-\frac{1-y^3}{3}\right)\left[h(0)-\int_0^1\frac{h(y)-h(0)}{y^2}dy\right]$$
$$+\frac{2w}{\pi}\int_0^1 h(y')\left[\frac{y^4-1}{2(1-y'^2)}+2-2y-y'\ln\left|\frac{(1+y')(y-y')}{(1-y')(y+y')}\right|\right]dy', \tag{13}$$

$h(y)$ clearly is a linear function of $s$. Note that because $y = 1$ when $x = 0$, $h(1) = 0$ and that $(1-\epsilon)h(0)$ is given by (9*b*). With $s$ fixed, (13) determines $h(y)$ in terms of the parameter $w$ alone. Thus, it is convenient mathematically to solve (13) with $w$ given and then to find the corresponding $\epsilon$ from (9*b*) and (11). (Physically, one would think of the contact angle hysteresis, $\epsilon$, as the given which then determines the critical Weber number, $w$.)

We also write $P$, as determined by (11), in terms of $h$ as

$$P = (1-\epsilon)I(w), \tag{14}$$

where
$$I(w) = 1-s+\frac{2w}{\pi}\left[h(0)+\int_0^1\frac{(1-y^2)h(0)-h(y)}{y^2(1-y^2)}dy\right]. \tag{15}$$

All integrals have been written in convergent form.

The solution to (13) and (15) will be expanded in powers of $w$ as

$$h(y) = \sum_0^\infty w^n h_n(y), \quad I = \sum_0^\infty w^n I_n. \tag{16}$$

Clearly
$$h_0 = \tfrac{1}{2}(1-y^4)+\tfrac{1}{2}s(1-y^2)^2, \quad I_0 = 1 \tag{17}$$

and $h_1$ could be found simply in closed form.

A finite truncation of (16) was evaluated by numerical integration. If (13) is written symbolically as

$$h(y) = \tfrac{1}{2}(1-y^4)+\tfrac{1}{2}s(1-y^2)^2+w\mathrm{L}(y;h), \tag{18}$$

| $n$ | $h_n(0)$ | $\frac{h_n(0)}{h_{n+1}(0)}$ |
|---|---|---|
| 0 | 0.500 | 0.707 |
| 1 | $0.707 \times 10^{-1}$ | 4.81 |
| 2 | $0.147 \times 10^{-1}$ | 4.48 |
| 3 | $0.328 \times 10^{-2}$ | 4.40 |
| 4 | $0.746 \times 10^{-3}$ | 4.39 |
| 5 | $0.170 \times 10^{-3}$ | 4.37 |
| 6 | $0.389 \times 10^{-4}$ | 4.37 |
| 7 | $0.891 \times 10^{-5}$ | 4.37 |
| 8 | $0.204 \times 10^{-5}$ | 4.37 |
| 9 | $0.467 \times 10^{-6}$ | 4.37 |
| 10 | $0.107 \times 10^{-6}$ | — |

TABLE 1. Coefficients in the Taylor series for $h(0)$ and the convergence of their ratio

where $\mathrm{L}(y;\bullet)$ represents the operation on the right-hand side of (13), then

$$h_n = \mathrm{L}(y; h_{n-1}) \quad (n \geqslant 1). \tag{19}$$

This expression was evaluated recursively with the integrals on the right-hand side being computed numerically.

Note that if a solution to the eigenvalue problem

$$\mathrm{L}(y; h_e) = \lambda^{-1} h_e^{(y)} \tag{20}$$

exists with $\lambda > 1$, then it is likely that the iterative solutions to (19) will converge to a constant times $\lambda^{-n} h_e(y)$, when $n \to \infty$. In this event, $\lambda$ is the radius of convergence to (16) and information about the infinite series can be surmised from the numerical solution for a finite number of terms. Our numerical analysis suggests that (20) has a solution with $\lambda = 4.37$: the evidence is presented in table 1 and figure 2. Table 1 shows numerical values of $h_n(0)$ for $n < 11$ and the ratio of $h_n(0)$ to $h_{n+1}(0)$ for the case $s = 0$. It is seen that the latter ratio converges rapidly to 4.37. Values in the table are rounded to 3 decimal places because this was the accuracy of the numerical integrations. Figure 2 shows numerical solutions for $h_n(x)/h_n(x = 1)$ (recall that $x = 1$ when $y = 0$). The curves for $n = 8$ and $n = 10$ lie almost atop one another, showing rapid convergence of the normalized $h_n(x)$ to $h_e(x)$. The coefficient of $s$ in the solution for $h_n(x)$ also shows rapid convergence to a multiple of the same function $h_e(x)$, as is shown by figure 2(*b*).

Once $h(y; w)$ has been computed, the contact angle hysteresis is found from (9*b*) with (14):

$$\epsilon = \frac{(2h(0)I + s^2)^{\frac{1}{2}} - 1}{(2h(0)I + s^2)^{\frac{1}{2}} + 1}. \tag{21}$$

For example, it is readily calculated using (17) that

$$h(0) = \tfrac{1}{2} + \tfrac{1}{2}s + \frac{2w}{9\pi} + \frac{sw}{9\pi} + O(w^2),$$

$$I = 1 - s + \frac{2sw}{\pi} + O(w^2),$$

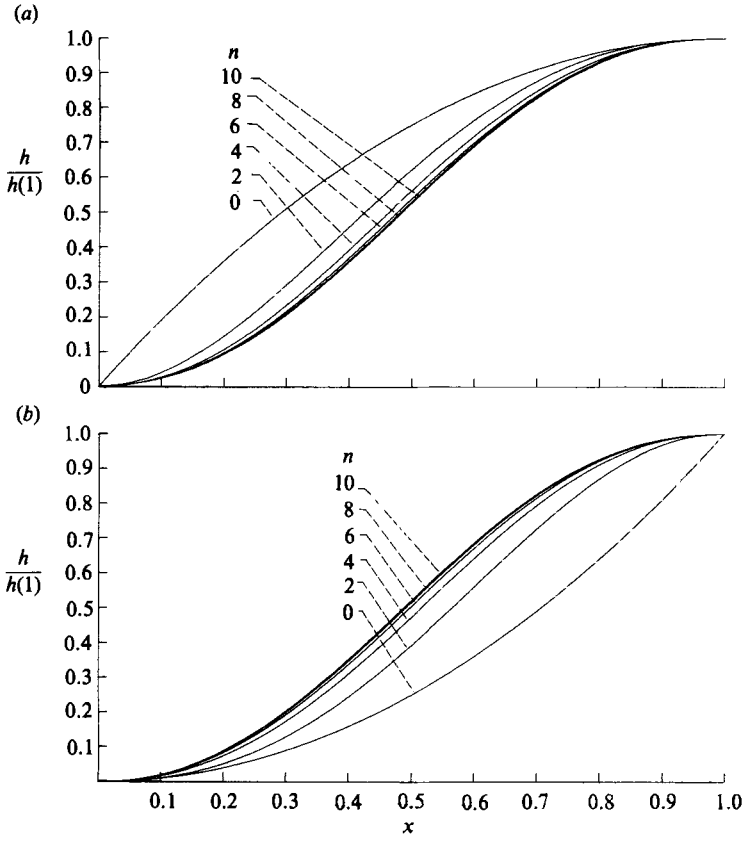


FIGURE 2. The even terms in the series (15) up to $n = 10$. This figure shows the rapid convergence to the eigensolution of (20). (*a*) is for $s = 0$ and (*b*) is the function which $s$ multiplies.

so one finds

$$\epsilon = (1+4s+4s^2)\frac{w}{9\pi} + O(w^2), \tag{22}$$

when $w \to 0$. This shows that when $s = -0.5$, $\epsilon$ vanishes to the level of approximation given. From (A 6) of the Appendix it follows that the drag on the drop vanishes for this value of $s$. Such occurrence signifies that the assumption of a free-streamline wake extending to downstream infinity cannot be maintained; for values of $s$ less than $-0.5$ the wake must be closed (Cheng & Smith 1982). For general values of $w$ the drag vanishes at some value of $s$, which is the minimum separation slope for which an infinite wake can be maintained.

One sees by figure 2 that if one writes $h = h_1 + sh_2$ the terms in the series (equation (16)) for $h_1$ and $h_2$ are all positive, so from the discussion below equation (20), $h(0; w)$ and $I(w)$ diverge like $(w-\lambda)^{-1}$ at $w = \lambda$. Then

$$\epsilon = 1 + O(w-\lambda) \tag{23}$$

when $w \to \lambda$. As a consequence of (23), $(1-\epsilon)$ times $I$ or $h$ is finite when $w \to \lambda$, and therefore $P$ and $\eta$ remain bounded at $w = \lambda$. Hence, the radius of convergence is where the contact angle hysteresis becomes unity, so that the receding contact angle is zero, and all physical variables are finite there. Because the receding contact angle must be greater than zero, $\lambda$ is the maximum value which a critical Weber number

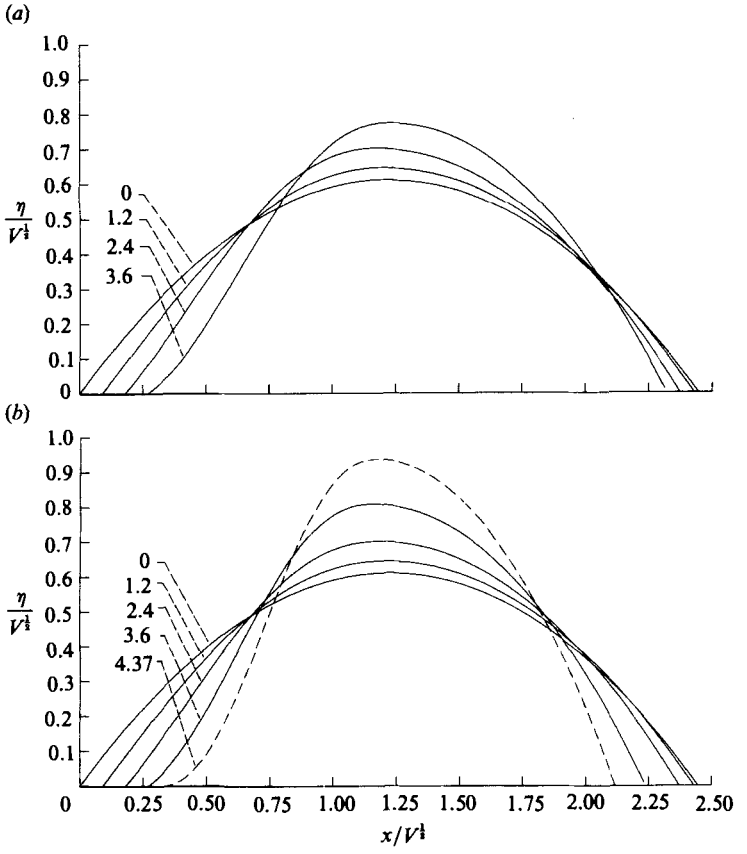


FIGURE 3. Drop shape, scaled to have unity volume, for values of $w$ labelled, calculated by summing 11 term Taylor series. ($a$) is simply a sum of the 11 terms. ($b$) is calculated using the approximation (equation (24)) to a sum of the infinite series. The dashed line shows the asymptotic drop shape at the radius of convergence, $w = 4.37$.

can take. Thus, we have the surprising result that when $\epsilon \to 1$, the critical Weber number becomes independent of $s$. This occurs because at the radius of convergence, the operator L in (18) dominates the non-homogeneous term. The eigenfunction has zero slope at separation, so the convergence of $\eta$ to $\eta_e$ is non-uniform in a small region around separation.

## 4. Results

### 4.1. *The case* $s = 0$

When $s = 0$ separation occurs at the top of the drop. One might expect that for large drops, separation takes place near the top. Of course, this intuition is based on drops to which the slender-body approximation would not apply. Nevertheless, the case $s = 0$ serves to illustrate the present solution. Results for other values of $s$ are presented later.

The drop shape was computed for various $w$ by summing 11 terms in the series (equation (16)) using the numerical evaluations of $h_n$ displayed in figure 2 (plus those for odd $n$), with amplitudes given in table 1: the result is plotted in figure 3($a$). The

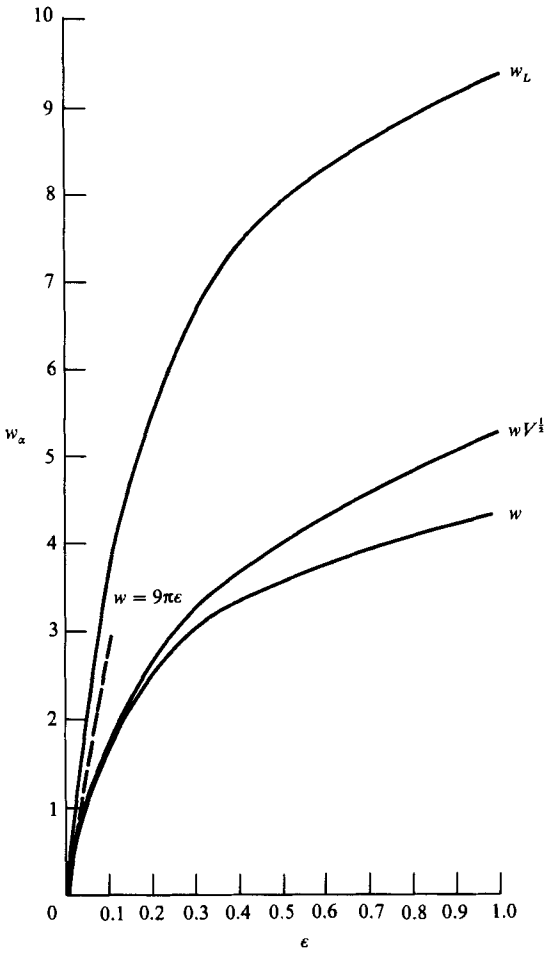


FIGURE 4. Critical Weber number versus contact angle hysteresis.

numerical integrations required to solve (19) were done by the trapezoidal rule with $\Delta y = \frac{1}{180}$. In principle, the rapid convergence of $h_n$ to $h_e$ permits an approximate evaluation of the infinite series (equation (15)):

$$h \approx \sum_0^9 w^n h_n(y) + \frac{w^{10} h_{10}(y)}{1 - w/\lambda}. \tag{24}$$

This improved formula was used in figure 3 (*b*). It is seen that the last term in formula (24) becomes significant in the case with $w = 3.6$. The dashed curve in figure 3 (*b*) shows the asymptotic shape when $w \to \lambda$. This shape is approached for non-zero values of $s$ as well.

Figure 3 is normalized so that all curves have unity area (also recall the scaling, equation (2)). The origin of each curve has been shifted to $x = 0.075w$ solely for the purpose of display. Beginning with the symmetric shape when $w = 0$, increasing wind speed increases asymmetry. Because the airflow stagnates on the front edge of the drop, $P_a$ is high there and the droplet curvature becomes negative (actually, the curvature has a logarithmic singularity at $x = 0$, in consequence of the slender-drop approximation). Proceeding over the drop, the air accelerates, producing suction

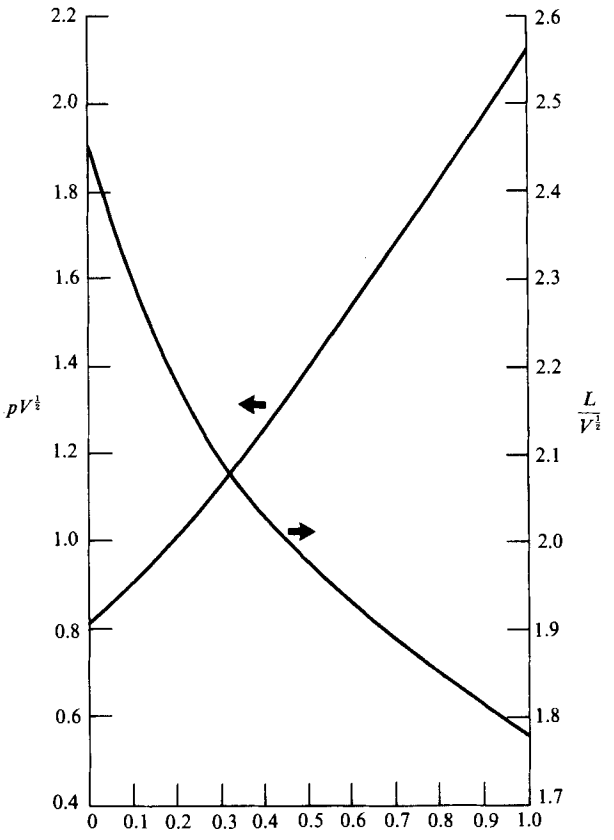


FIGURE 5. Internal drop pressure and drop length versus contact angle hysteresis.

(relative to the internal pressure) at the crest of the drop; hence, the crest is drawn up. The leeward side of the drop is simply a constant curvature segment, given by expression (9*a*).

Equation (21) was used to evaluate the contact angle hysteresis as a function of critical Weber number. For this purpose, an 11 term expansion for $h(0; w)$ and $I(w)$ was used, with a correction for the rest of the infinite series as in the summation formula (equation (24)). Once $\epsilon$ was calculated for a given $w$, equations (8), (10) and (14) were used to evaluate $V$, $L$, and $P$.

In figure 4 we show the resultant curves of Weber number versus $\epsilon$. Three forms of Weber number are shown, differing in the lengthscale used: $w$ is based on the distance to separation; $w\,V^{\frac{1}{3}}$ is based on drop volume; and $w_L = w\,L$ is based on drop length. Equation (22) gives the asymptotic behaviour $w \to 9\pi\epsilon$ when $\epsilon \to 0$, and this is shown in the figure. Also $V \to \frac{2}{3}$ and $L \to 2$ when $\epsilon \to 0$, which determines the behaviour of the other curves near the origin. It is seen that the small $\epsilon$ approximation is reasonably accurate for $w < 0.8$, but this corresponds to $\epsilon < 0.03$, so the approximation is applicable only to quite small contact hysteresis.

From the numerical series, reasoning as in equation (24), we find that as $w \to \lambda = 4.37$,

$$h(0) \to \frac{0.27}{\left(1-\frac{w}{4.37}\right)}, \quad I \to \frac{0.42}{\left(1-\frac{w}{4.37}\right)}, \tag{25}$$

approximately. Hence,

$$1-\epsilon \to 4.15\left(1-\frac{w}{4.37}\right).$$

Figure 5 shows that with increasing contact angle hysteresis, the internal pressure at critical conditions rises and the scaled length of the drop decreases (i.e. its thickness increases). The increased thickness is consistent with the crest of the drop being drawn up by suction, but the increase of $P$ might be surprising. Presumably, the low pressure at the crest is balanced primarily by surface tension through increased curvature, while the rise of internal pressure largely balances the high air pressure in the stagnation region. Ostensibly, this latter is why the curvature is not more negative on the front of the drop.

If one places a drop of water on a sheet of glass and blows tangentially to the surface, the drop is distorted towards the shape shown by the dashed line in figure 3. One sometimes observes that the drop has a thin tail on the upstream side. When the drop contracts from its initial length, as the wind begins to blow, the downstream side remains fixed and the upstream side moves downstream. The tail, then, is a residue left behind during this contraction and the bulk of the drop is as in figure 3. One also sometimes observes temporal oscillations of the drop surface. These are likely to be due to a shear flow instability of the separated wake (R. J. Hansman and S. R. Turnock, private communication 1987).

### 4.2. *Other values of s*

Figures 6(*a*), (*b*) and (*c*) show evaluations of critical Weber numbers versus contact angle hysteresis for various values of $s$. When $\epsilon \to 0$, $L \to 2/(1-s)$, which becomes large when $s \to 1$. This is why the curve in figure 6(*b*) with $s = 0.75$ crosses that with $s = 0.5$ at small $\epsilon$. Recall that $s$ is the separation angle divided by the receding contact angle. Thus when $\epsilon \to 0$, were $s = 1$, separation would occur at the leading edge of the drop; but then the drop would lie entirely within the constant pressure separated region, and the wind would be unable to dislodge the drop.

Because lengths were normalized by $x_s$, when the separation point moves to the leading edge, $L \to \infty$ and $P \to 0$. For general values of $\epsilon$, the criterion $P = 0$ gives the maximum value which $s$ can take: for small $w$, setting $I = 0$ above (22) gives this maximum. In discussing Brillouin point separation in §5, it will be seen that a more stringent upper bound on $s$ exists. As discussed in connection with (22), a minimum slope exists for which the wind drag, and hence $\epsilon$ vanishes. In figure 6 this slope is determined as a function of Weber number by the intersections of the curves with the $\epsilon = 0$ axis. For the present analysis to be valid $s$ must lie between these minimum and maximum values.

In order to illustrate the dependence of drop shape on $s$, we include in figure 7 curves of $\eta(x/V^{\frac{1}{2}})/V^{\frac{1}{2}}$ for $s = -0.5$, 0 and 0.5 with $w = 3$.

When the Weber number is less than critical, the present analysis would describe the deformation of the drop by air flow. In this case, the leading edge ($\theta(0)$) and trailing edge ($\theta(L)$) angles would have to be determined as functions of $w$. Thus, instead of determining critical Weber number as a function of given contact angles, as done here, the contact angles would be determined as functions of a given Weber number. If $\epsilon$ is redefined below equation (6) with $\theta(0)$ and $\theta(L)$ replacing $\theta_R$ and $\theta_A$, the present analysis determines $\epsilon(w)$. In order to determine $\theta(0)$ and $\theta(L)$ individually, a further relation is required. The relation we propose is that the average of these angles be a fixed constant, equal to the previously defined $\bar{\theta}$. The reason for this proposal is as follows. If a drop is sitting on a flat plate oriented

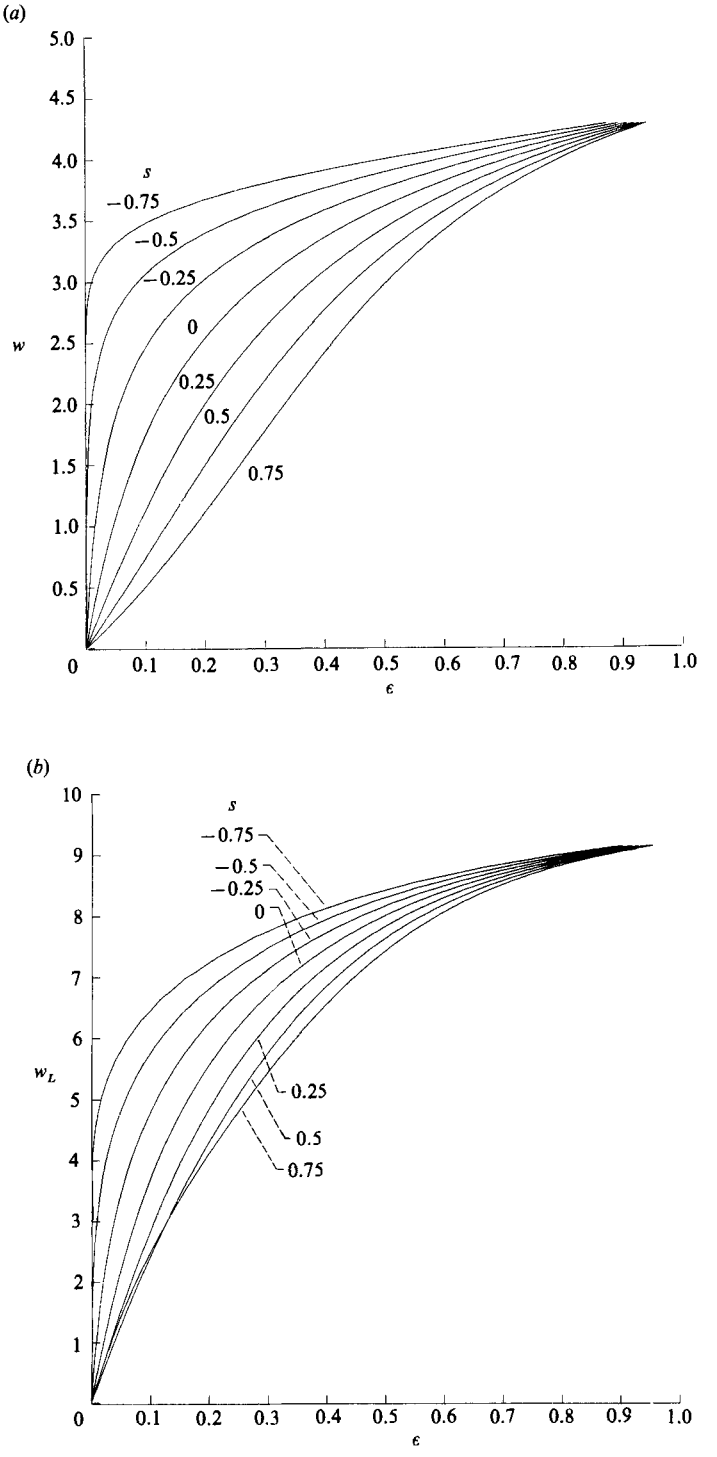


FIGURE 6(*a*, *b*). For caption see facing page.

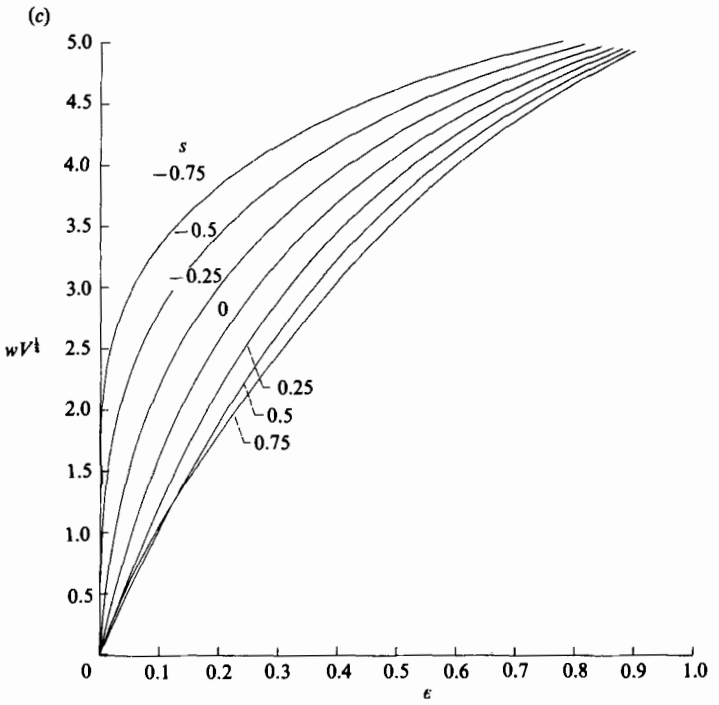


FIGURE 6. Critical Weber numbers versus contact angle hysteresis for values of $s$ labelled.

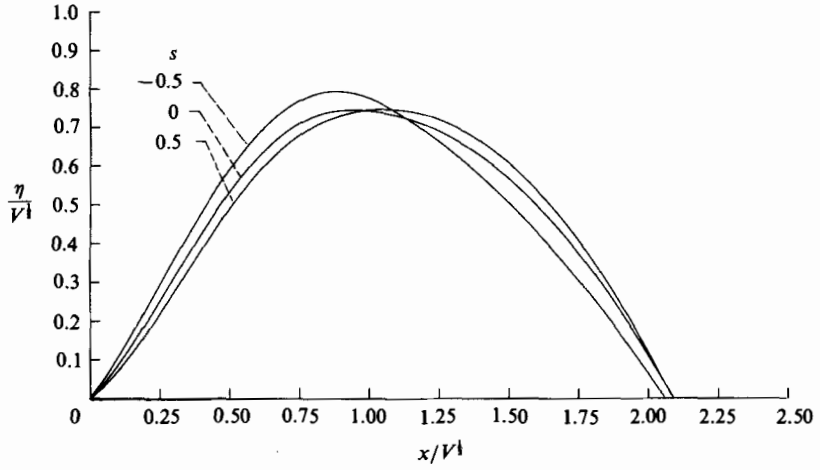


FIGURE 7. Comparison of drop shapes when $s = -0.5$, 0 and 0.5 for $w = 3$.

perpendicular to a gravitational field, the balance of forces on the drop surface, in the direction normal to the plate is

$$\sigma(\sin\theta(0) + \sin\theta(L)) = -PL + Mg, \tag{26}$$

where variables are dimensional and $M$ is the mass (per unit length) of the drop. If the plate is accelerated downward, $g$ is effectively reduced and the balance of forces can be maintained either through reduction of internal pressure, or through change

of contact angle. The traditional argument leading to the concept of contact angle (Batchelor 1967, §1.9) allows no dependence on gravity; surface tension forces are produced by molecular attraction. Thus, we propose that the left-hand side of (26) is unaffected by the applied force (which in the present paper is aerodynamic lift). This means that the normal component of the weight of the drop is supported entirely by the surface on which it rests, with no assistance from surface contact forces. This argument is clouded somewhat by the fact that the tangential component of weight must be supported by surface contact. In the slender-body limit, our hypothesis means that

$$\tfrac{1}{2}(\theta(0)+\theta(L)) = \bar{\theta}, \tag{27}$$

where $\bar{\theta}$ is a known constant.

## 5. Discussion on the relation to viscous theory

In §1, we commented on the ability of high-Reynolds-number viscous theory to provide a relation between the separation point and the thickness of the boundary layer approaching the drop. In general, the present analysis could be set in the context of viscous theory. To do so, lengths would be non-dimensionalized by the distance upstream of the drop over which the boundary layer grows; on a flat plate this would be the distance to the leading edge. The air-flow Reynolds number, $Re$, based on this length would be considered asymptotically large.

In addition to $Re$, the ratio, $\mu_a\nu_a/\mu_d\nu_d$, of kinematic times dynamic viscoscities of the air to the liquid enters the scaling. If this ratio is taken to be sufficiently small, the liquid motion is governed by the creeping flow equation, $-\mathrm{d}P/\mathrm{d}x = Re^{-1}\partial^2 u/\partial z^2$. If the drop height is sufficiently large, the viscous term cannot balance a lowest-order pressure gradient, so the internal drop pressure must be constant.

If the drop height is reduced, pressure gradient and viscous forces can become comparable. However, because the viscous stress is continuous across the drop surface, these forces are also in balance within a region comparable to the drop height in the air flow over the drop. This means that viscous displacement of the boundary-layer flow over the drop by the secondary boundary layer generated on the drop, is comparable to geometrical displacement by the drop height. But this is precisely the condition that leads to an interactive boundary layer. Thus, the case in which viscous stresses contribute equally with pressure forces to dislodging the drop, is that in which the boundary layer also becomes interactive. The triple-deck theory (Smith *et al.* 1981) provides a systematic derivation of nonlinear equations governing this case. Thus, the drop length would be taken to be $O(Re^{-\frac{3}{8}})$ and $\bar{\theta}$ would be $O(Re^{-\frac{1}{4}})$ as $Re \to \infty$. In order for surface tension to balance the normal force jump across the drop surface, the Weber number based on distance to the leading edge must be $O(Re^{\frac{3}{8}})$; correspondingly, the Weber number based on drop dimensions would be $O(1)$.

Smith *et al.* (1981) speculate that in the large height limit (or large drop volume limit presently) the free-streamline, slender-body theory emerges from the nonlinear triple-deck problem, with a definite separation point. For the present drop problem, surface tension forces contribute to determining this separation location.

Cheng & Smith (1982) describe an alternative scenario (which could be that which emerges from the triple-deck limit) in which the separation location on a slender body is determined by high-Reynolds-number viscous theory. In their sealing, the drop length would be $O(1)$ and $\bar{\theta}$ would be $O(Re^{-\frac{1}{16}})$. The separation now is provoked by viscous effects in a triple-deck region around the separation point, with length of

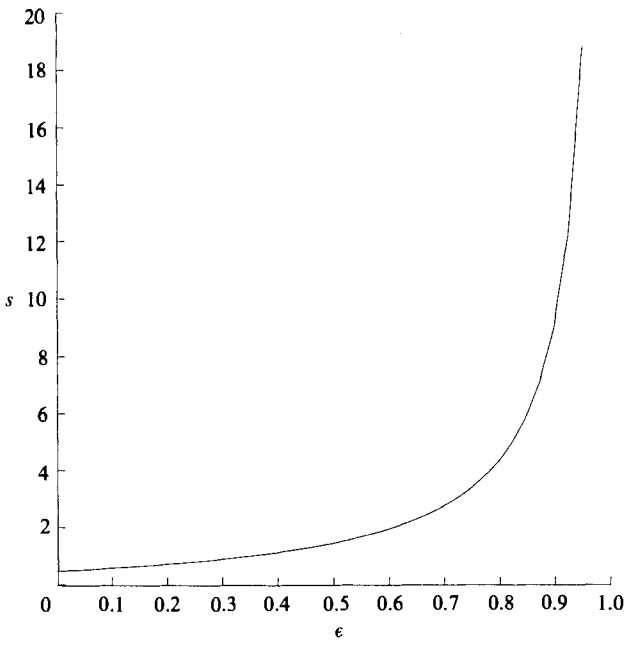


FIGURE 8. Slope at separation versus contact angle hysteresis for Brillouin point separation.

$O(Re^{-\frac{3}{8}})$. In this event, surface tension forces can play no role in the separation. Cheng & Smith's equation (3.2*c*) provides a linear relation between $s$ and the parameter

$$\pi\beta\lambda_{\mathrm{b}}^{\frac{9}{8}} Re^{-\frac{1}{16}} \frac{x_{\mathrm{S}}^{\frac{1}{2}}}{d^{\frac{1}{2}}\theta_{\mathrm{R}}}, \tag{28}$$

where $\beta$ and $\lambda_{\mathrm{b}}$ are constants and $d$ is the distance to the leading edge of the boundary layer. Through the dependence on $d$, this relation permits $s$ to vary over a range of values, as we have allowed it to do. However, a new feature now arises: we found that the coefficient of $s$ in Cheng & Smith's equation vanished when $w \approx 3.3$. At this value of $w$, $s$ becomes infinite, $\epsilon$ becomes unity, and all physical variables remain finite. Hence, 3.3 becomes a new maximum critical Weber number, which is attained for liquid, solid interfaces with zero receding contact angle.

The separation point ambiguity also could be removed by the classical Brillouin criterion (Sychev 1972) if $O(1)$ drops, to which the slender-body approximation no longer applies, are considered. The Brillouin criterion is that the separation is at that point for which the pressure gradient is not singular. In general the fully nonlinear equations for the free-streamline, and drop curvature, must be solved, but in the case of thin drops, the slender-body equations emerge. In this case, to lowest order in $Re^{-1}$, the thickness of the upstream boundary layer has no influence on the location of separation. However, Sychev (1972) showed that viscous effects can cause the separation point to move an $O(Re^{-\frac{1}{16}})$ distance from the Brillouin point; for practical Reynolds numbers, this is effectively an $O(1)$ distance, so the Brillouin criterion is not compelling. Nevertheless, it provides a unique and reasonable location for the separation point. The Brillouin condition is invoked by choosing $s$ such that the integral in (A 4) vanishes at $x = 1$, thereby making the pressure gradient non-singular (for small $w$ this gives $s = 0.5$). The resulting values of $s$ versus $\epsilon$ are

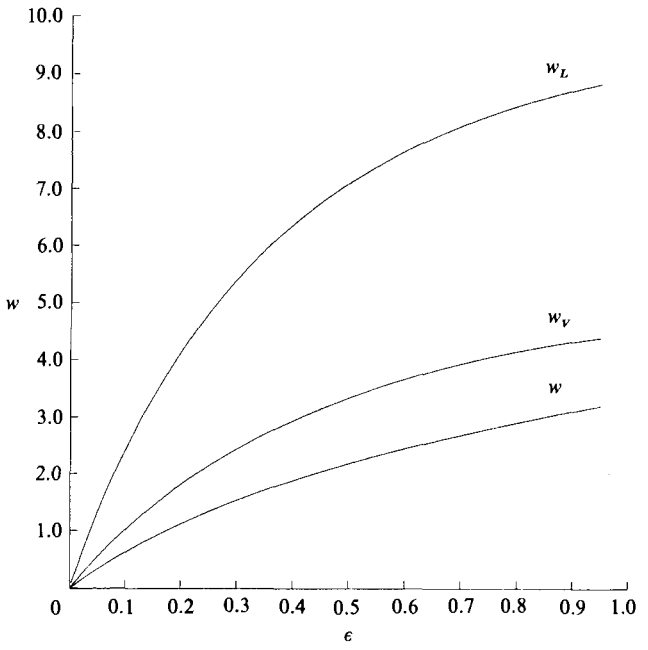


FIGURE 9. Critical Weber numbers for Brillouin point separation.

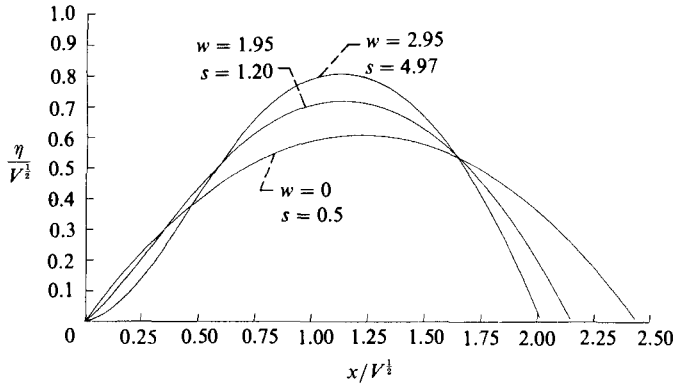


FIGURE 10. Drop shapes for Brillouin point separation for Weber numbers shown.

presented in figure 8. On this curve $L$ is finite, and in fact decreases from its value of 4 as $s$ increases from 0.5. Because the drag is also positive, these separation slopes lie within the acceptable range. When $w \to 3.3$, $s \to \infty$ and $\epsilon \to 1$, as was discussed previously. Curves of critical Weber number for Brillouin point separation are displayed in figure 9.

In the classical free-streamline theory, it is observed that were the separation point upstream of the Brillouin point, the free-streamline would enter the surface. In the present case, in order to avoid this, at each value of $\epsilon$ acceptable values of $s$ must be less than those shown in figure 8. (Note that the curve for $s = 0.75$ in figure 6 is therefore invalid at the smallest values of $\epsilon$.)

Figure 10 illustrates droplet shapes for a few cases of Brillouin point separation.

## Appendix. The formula for $P_a$

We wish to derive the surface pressure associated with free-streamline separation in the slender-body limit. This could be done by invoking the full free-streamline theory (Milne-Thompson 1968 §12.40 ff.) and linearizing the conformal mapping. However, the method described below produces the same result. Hence, it describes the situation depicted in figure 1 in the slender-body limit. The flow outside the wake is irrotational and the wake is bounded by a vortex sheet.

External to the separation region, the air motion is given by potential flow. Thus, in the slender-body approximation the air pressure satisfies Laplace's equation. If $z$ is the coordinate normal to the surface, the condition of flow tangency and the $z$-momentum equation give the boundary condition,

$$\frac{\partial P_a}{\partial z} = \begin{cases} -w\dfrac{d^2\eta}{dx^2} & (0 \leqslant x \leqslant 1), \\ -w\dfrac{d^2\eta_s}{dx^2} & (x \geqslant 1), \end{cases} \tag{A 1}$$

where $z = \eta_s(x)$ is the equation of the separation streamline. The boundary value of the harmonic function satisfying (A1) and tending to zero as $z$ tends to infinity, is (Muskhelishvili 1946)

$$P_a = \frac{w}{\pi}\int_0^1 \frac{\dfrac{d\eta(x')}{dx'}}{x'-x}dx' + \frac{w}{\pi}\int_1^\infty \frac{\dfrac{d\eta_s(x')}{dx'}}{x'-x}dx'. \tag{A 2}$$

The condition of free-streamline separation, $P_a = 0$; $x > 1$, applied to (A 2) provides an integral equation for $\eta_s(x)$. If tangential separation, $d\eta_s(1)/dx = d\eta(1)/dx$, is required, then the solution for $\eta_s(x)$ is

$$\frac{d\eta_s}{dx} = \frac{-(x-1)^{\frac{1}{2}}}{\pi}\int_0^1 \frac{\xi(x')dx'}{(1-x')^{\frac{1}{2}}(x'-x)} \quad (x \geqslant 1), \tag{A 3}$$

in the notation of (3). The alternative to the coefficient of the integral having a square root zero is a square root singularity, which is unacceptable.

When (A 3) is substituted back into (A 2) is it found that

$$P_a = 0 \quad (x \geqslant 1), \tag{A 4}$$

$$P_a = \frac{w(1-x)^{\frac{1}{2}}}{\pi}\int_0^1 \frac{\xi(x')dx'}{(1-x')^{\frac{1}{2}}(x'-x)} \quad (0 \leqslant x \leqslant 1).$$

The total wind drag, $D$, on the drop is

$$D = \frac{\rho U^2\bar{\theta}^2}{w}\int_0^1 \xi P_a\,dx = \frac{\rho U^2\bar{\theta}^2}{2\pi}\left(\int_0^1 \frac{\xi(x)dx}{(1-x)^{\frac{1}{2}}}\right)^2. \tag{A 5}$$

Upon multiplying (3) by $\xi$ and integrating from $x = 0$ to $L$, it is found that

$$D = \frac{1}{2}\frac{\rho U^2}{w}\left(\theta_A^2 - \theta_R^2\right) = 2\frac{\rho U^2\bar{\theta}^2}{w}\epsilon. \tag{A 6}$$

For non-slender drops, $\theta_A^2$ and $\theta_R^2$ would be replaced by $-2\cos\theta_A$ and $-2\cos\theta_R$.

## REFERENCES

BATCHELOR, G. K. 1967 *An Introduction to Fluid Dynamics*. Cambridge University Press.

CHENG, H. K. & SMITH, F. T. 1982 *Z. angew. Math. Phys.* **33**, 151–180.

DUSSAN, V. E. B. 1987 *J. Fluid Mech.* **174**, 381–397.

MILNE-THOMPSON, L. M. 1968 *Theoretical Hydrodynamics*, 5th edn. Macmillan.

MUSKHELISHVILI, N. I. 1955 *Singular Integral Equations*, 2nd edn. Gronigen: P. Noordhoff.

SMITH, F. T. 1977 *Proc. R. Soc. Lond.* A, **356** 443–463.

SMITH, F. T., BRIGHTON, P. W. M., JACKSON, P. S. & HUNT, J. C. R. 1981 *J. Fluid Mech.* **113** 123–152.

SYCHEV, V. V. 1972 *Fluid Dyn.* **7** 407–417.